Effect of Zirconia Doping on the Structure and Stability of CaO−Based Sorbents for CO2 Capture during Extended Operating Cycles

ARTICLE *in* THE JOURNAL OF PHYSICAL CHEMISTRY C · NOVEMBER 2011

Impact Factor: 4.77 · DOI: 10.1021/jp207625c

4 AUTHORS:

Rajesh Koirala
ETH Zurich
8 PUBLICATIONS **92** CITATIONS
SEE PROFILE

Krishna Reddy Gunugunuri
Toyota Research Institute of North America
52 PUBLICATIONS **725** CITATIONS
SEE PROFILE

Sotiris E. Pratsinis
ETH Zurich
501 PUBLICATIONS **16,427** CITATIONS
SEE PROFILE

Panagiotis G Smirniotis
University of Cincinnati
146 PUBLICATIONS **5,231** CITATIONS
SEE PROFILE

THE JOURNAL OF PHYSICAL CHEMISTRY C

ARTICLE

pubs.acs.org/JPCC

Effect of Zirconia Doping on the Structure and Stability of CaO-Based Sorbents for CO_2 Capture during Extended Operating Cycles

Rajesh Koirala,[†] Krishna R. Gunugunuri,[†] Sotiris E. Pratsinis,[‡] and Panagiotis G. Smirniotis*[,†]

[†]Chemical Engineering Program, School of Energy, Environmental, Biological, and Medical Engineering, University of Cincinnati, Cincinnati, Ohio 45221-0012, United States

[‡]Particle Technology Laboratory, Department of Mechanical and Process Engineering, ETH Zurich, CH-8092 Zürich, Switzerland

ABSTRACT:

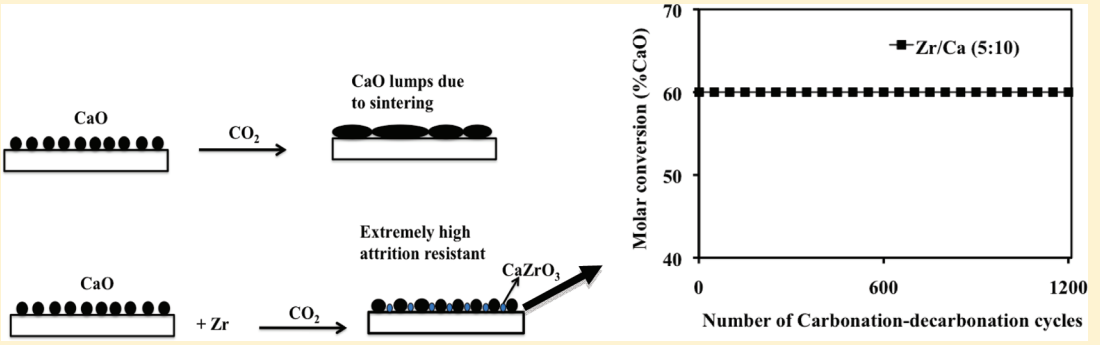

A series of CaO-based sorbents are made using flame spray pyrolysis (FSP) and doped in situ by a wide range of zirconia loadings and tested for their CO_2 capture during extended operating cycles. Among all these sorbents, the one with a Zr/Ca molar ratio of 5/10 exhibits optimum performance and remarkable stability up to 1200 cycles. That sorbent exhibited excellent resistance toward high temperature sintering under severe conditions. Its mechanical durability is attributed to the formation of well-dispersed $CaZrO_3$ nanoparticles that act as a barrier against sintering, preventing CaO grain growth. X-ray diffraction (XRD) revealed the formation of $CaCO_3$ and $CaZrO_3$ in all sorbents made here. The peak intensity of the perovskite-structured $CaZrO_3$ stabilizes at a molar ratio of Zr/Ca = 5/10. With increasing Zr doping, the $CaZrO_3$ size decreases, the specific surface area and pore volume increase, while the major TPD desorption peak shifts to a lower temperature. Both Ca2p and Zr3d electron binding energies decrease with increasing Zr content up to 5 mols of Zr doping and remained constant beyond that. Also, XPS of the O1s electron binding energies suggests that there are two types of oxygen, one from CaO and another from $CaZrO_3$. Surface enrichment of Zr of the Zr/Ca (6/10) sorbent explains the sharp drop in CO_2 capture capacity compared to that of the Zr/Ca (5/10) sorbent. With the reduction of $CaZrO_3$ size and fine-tuning of the Zr/Ca molar ratio, stable sorbents can be obtained for a very large number of cycles, while preserving relatively high CaO molar conversions (as high as 60%).

1. INTRODUCTION

The continuous increase in demand for energy from fossil fuels leads to higher CO_2 emissions. Capture technologies such as amine-based adsorbents and membranes are used for CO_2 removal from process gas streams. However, these technologies complicate the operation due to the need of monitoring numerous process parameters, high operating costs, and low performance.[1,2] However, sorbent-based technology can overcome these complications and maintain superior performance even in adverse environments.[3−7] Among all proposed sorbents, calcium oxide-based (CaO) sorbents derived from readily available natural minerals are well-known for high temperature CO_2 capture at low cost. The reversible reaction for CO_2 capture by CaO is

$$CaO(s) + CO_2(g) \leftrightarrow CaCO_3(s) \quad (1)$$

The sorption capacity and regenerability of the pure sorbent have suffered significantly due to sintering during multicyclic operation.[3,5,7] This reduction in activity is associated with an increase in CaO grain size and formation of a $CaCO_3$ layer on the sorbent surface that inhibits CO_2 diffusion and capture. Numerous methods such as pore structure modification, steam reactivation, and novel metal doping have been proposed to improve the performance of CaO-based sorbents. Arias et al.[4] used steam to reactivate the CaO sorbent in the hydrator. They found that steam is more efficient when a small fraction of sorbents is hydrated to a higher degree. Manovic and Anthony[5] were able to

Received: August 8, 2011
Revised: November 8, 2011
Published: November 10, 2011

improve the sorption cyclic performance of the CaO sorbent using steam reactivation to increase the sorbent pore volume.

An alternative approach was to incorporate refractory metal(s) on CaO to improve the CO_2 capture capacity and its resistance to sintering.[6−9] Martavaltzi and Lemonidou[6] developed CO_2 sorbents composed of CaO and $Ca_{12}Al_{14}O_{33}$ with a capture capacity higher than 6 mol kg^{-1} of sorbent even after 45 carbonation−decarbonation cycles. This enhancement in sorbent stability was attributed to $Ca_{12}Al_{14}O_{33}$ that inhibited sintering of CaO by providing a stable framework. Li et al.[7] also investigated CaO-based sorbents, namely, $CaO/Ca_{12}Al_{14}O_{33}$, in mild as well as severe calcination conditions. The sorbent attained 41 wt % and 22 wt % CO_2 capture capacity after 50 and 56 cycles under mild and severe calcination, respectively. Similarly, Aihara et al.[8] used titania to create an inert framework of $CaTiO_3$ to stabilize the sorbent performance during cyclic operation. But none of them exhibited satisfactory results, especially during prolonged cyclic carbonation−decarbonation operations under both mild and severe conditions.

A variety of metal dopants (M = Cr, Si, Ti, Co, Zr, and Ce) for CaO (spinel lattice) have been introduced and screened for their effectiveness in CO_2 capture capacity and stability.[9] Among these sorbents, the Zr/Ca (3/10) sorbent exhibited high performance and excellent stability up to 100 cycles when tested under 30 vol % CO_2. The sorbent maintained its superior performance under severe operating conditions involving the introduction of 10 vol % of water vapor into the feed stream. In the present study, the goal is to find the optimum Zr doping into the CaO lattice for maximum capture capacity and stability during extended operation cycles. For this purpose, sorbents of various Zr/Ca molar combinations are made by flame spray pyrolysis (FSP).[9] They are characterized by various methods, and their capacity and stability are evaluated up to 1200 cycles.

2. EXPERIMENTAL SECTION

2.1. Sorbent Preparation. *2.1.1. Flame Spray Pyrolysis (FSP).* The experimental procedure is explained in detail by Lu et al.[9] Therefore, in the present study, a calcium-naphthenate precursor (4% calcium in mineral spirits) and Zirconyl (IV) 2-ethylhexanoate (6% Zr in mineral spirit), both from Strem Chem Inc., were dissolved in xylene (Reagent ACS). A wide range of precursor solutions were prepared having Zr/Ca molar ratios from 1:20 to 6:10. The freshly prepared precursor solution was injected at 1−2.5 mL min^{-1} by a syringe pump (Cole-Parmer) through the spray nozzle and dispersed by 5 L min^{-1} of oxygen (Wright Bros, Inc.) into a fine spray. The pressure drop of dispersion O_2 was maintained at 1.5 bar at the nozzle tip. The combustion of the fine spray was initiated and maintained by the ignition of premixed 500 mL min^{-1} of CH_4 and 400 mL min^{-1} of O_2. The product powders were collected on a flat glass fiber filter (GF/D Whatmann, 25.7 cm in diameter) placed on a holder above the reactor with the aid of a vacuum pump (Grainger, Inc.). For the present basic research, high purity and quality precursors have been used to avoid unexpected and uncontrolled performance. For industrial synthesis of such sorbents, slightly different FSP designs permit the use of C_2H_2 and ethanol rather than the present expensive ethylhexanoate-based precursors and solvents.[10]

2.1.2. Physical Mixing Method. A wide range of sorbents was prepared by mixing predetermined quantities of commercially available CaO (JT Baker Reagents) and $CaZrO_3$ (Alfa Aesar). The resultant mixture of sorbents was properly blended to ensure perfect mixing after which it was calcined in air at 750 °C for 1 h (with ramp rate of 5 °C min^{-1}) before analyzing in TGA.

2.2. Characterization. *2.2.1. XRD.* X-ray diffraction (XRD) of all CaO-based sorbents was conducted on a Phillips X'pert diffractometer using Cu Kα (1.54056 Å) as the radiation source. The intensity data were collected over a 2θ range of 20−80° with a step size of 0.05° and with a scanning rate of 1 s/point. Crystalline phases were identified through comparison to reference data from the International Centre for Diffraction Data (ICDD) files. The crystallite size of $CaZrO_3$ was estimated by the Debye−Scherrer equation.[11] Validation was done by comparing the XRD spectra of the Zr/Ca (3/10) sorbent to that made earlier.[9] To confirm the phase purity, XRD of the sorbents was performed on two other diffractometers, Siemens D500 and Rigaku D-2000. All measurements showed similar patterns and intensities.

2.2.2. Temperature Programmed Desorption (TPD). TPD analysis of CO_2 on all CaO-based sorbents was conducted on Micromeritics AutoChem 2910. All samples were heated up to 800 °C at a ramp rate of 1 °C min^{-1} to remove impurities and chemisorbed CO_2 and cooled to 100 °C in helium before proceeding with the analysis. Then, the pretreated samples were exposed to 60 mL min^{-1} of 30 vol % of CO_2 in helium for 1 h. To ensure the complete removal of physisorbed CO_2 from the sorbent, 30 mL min^{-1} of helium was passed over the sample for 3 h. The temperature was then increased to 800 °C with a ramping rate of 1 °C min^{-1} while simultaneously recording the CO_2 desorption from the sorbent.

2.2.3. BET Surface Area and Pore Size Distribution Measurement. All samples were pretreated at 300 °C for 3 h before analysis. The BET (Brunauer−Emmett−Teller) surface area and pore size distribution analyses were conducted by N_2 physisorption at −196 °C using a Micromeritics ASAP 2010 apparatus. The specific surface area (SSA) was calculated using the six-point N_2 adsorption isotherm recorded in a relative partial pressure (p/p_0) range of 0.05−0.25. The pore volume was calculated using a single-point adsorption value at the relative pressure of about 0.99.

2.2.4. TEM. Select fresh and spent samples were characterized with a Philips CM 20 electron microscope. The samples were sonically dispersed in ethyl alcohol and transferred onto a carbon-Cu grid. After complete evaporation of the alcohol, the particles attached on the walls of holes in the carbon film were examined. The applied accelerating voltage was 200 keV, with a LaB_6 emission current and a point-to-point resolution of 0.27 nm.

2.2.5. XPS. X-ray photoelectron spectroscopy (XPS) was performed on a Pyris VG thermo scientific spectrometer using Al Kα (1486.6 eV) radiation as the excitation source. The binding energy of the adventitious carbon (C 1s) was set at 284.6 eV to correct for sorbent charging. The samples were degassed under vacuum for four hours before analysis. The XPS analysis of degassed samples was performed at ambient temperature and pressures typically around 10^{-8} Torr.

2.3. Sorbent Performance Test. Sorbent analysis of the above FSP-made sorbents was performed with a Perkin-Elmer Pyris-1 thermogravimertic analyzer (TGA). The microbalance of the Pyris-1 TGA measures up to 0.1 μg. A small amount of sorbent (ranging from 2 mg to 8 mg) was placed in a platinum boat. Before the carbonation−decarbonation experiments, each sorbent was first pretreated up to 750 at a 10 °C min^{-1} ramp under helium for 30 min to remove all impurities and preadsorbed CO_2. All the sorbents were carbonated and decarbonated

Table 1. BET Specific Surface Area, Equivalent Particle Size, and Pore Volume As a Function of Precursor Feed Rate

precursor feed rate (mL min^{-1})	BET specific surface area (m^2/g)	pore volume (cm^3/g)	particle size (nm)
1	49	0.02	36
1.5	46	0.17	38
2	40	0.18	46
2.5	32	0.19	56

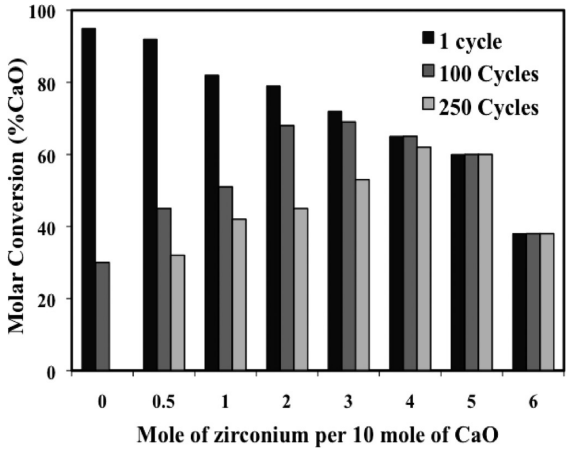

Figure 1. Effect of zirconia doping on molar conversion of CaO-based sorbents during extended operation cycles. The sorbents were carbonated with 20 mL min^{-1} of CO_2 (99.5%) and decarbonated with 20 mL min^{-1} of helium at 700 °C.

at 700 °C with 20 mL min^{-1} of CO_2 (99.5%, Wright Bros, Inc.) and with 20 mL min^{-1} of helium for 30 min alternatively. Gas flow rates were accurately monitored by Thermal Analysis Gas Station (Perkin-Elmer). The sorbent weight and temperature were recorded as a function of time during the entire analysis. Molar conversion (X_{CaO}%) of each sorbent was calculated by

$$X_{CaO}\% = \frac{W_{CaO}\%}{0.786} \times \frac{1}{\alpha_{CaO}} \quad (2)$$

where W_{CaO}% is the weight percentage change of the sorbent during CO_2 capture, 0.786 is the stoichiometric uptake of CO_2 by CaO, and α_{CaO} is the weight fraction of CaO present in the sorbent.

3. RESULTS AND DISCUSSION

3.1. Influence of Synthesis Conditions on Sorbent Properties. The product particle size can be controlled by the variation of precursors and oxygen dispersion gas flow rates.[12] The effect of precursor flow rates on CaO particle size is shown in Table 1. The average particle diameter calculated from BET analysis has been reduced from 52 to 36 nm by decreasing the precursor feed rate from 2.5 to 1 mL min^{-1}. The effect of precursor flow rate on particle size is consistent with flame synthesis of SiO_2,[12] ZnO,[13] and CeO_2.[14] The particle size increases with increasing precursor feed rate due to high concentration of CaO and high concentration of fuel within the flame spray resulting in high particle concentration and longer residence time at high temperatures.

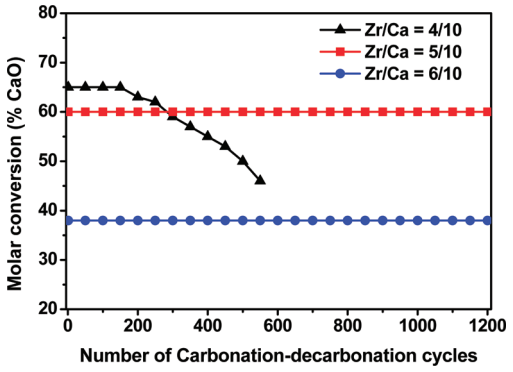

Figure 2. Stability and performance test of Zr/Ca (4/10, 5/10, and 6/10) sorbents during extended cyclic operation where the sorbents are carbonated with 20 mL min^{-1} of CO_2 (99.5%) and decarbonated with 20 mL min^{-1} of helium at 700 °C.

Therefore, particle size increases by sintering and agglomeration (coagulation). Here, the carbonation−decarbonation experiments were carried out with the sorbents synthesized with a precursor feed rate of 1.5 mL min^{-1} ensuring relatively small (~38 nm) particle size.

3.2. Sorbent Performance. The evaluation of all FSP-made zirconia-doped CaO-based nanosorbents at the carbonation−decarbonation temperature of 700 °C is presented in Figures 1 and 2. Extended operation cycles were performed on each nanosorbent to study its resistance toward sintering. Figure 1 compares the molar conversion of CaO-based sorbents doped with different mols of Zr at 1, 100, and 250 cycles. The pure CaO sorbent showed the highest uptake of about 95%. However, with increasing cycle number, its capacity dropped, reaching about 30% at the 100th cycle. This was attributed to nanoparticle sintering and the irreversible formation of a $CaCO_3$ layer outside the CaO core by prolonged exposure to elevated temperatures and a high concentration of CO_2. Sintering leads to lower sorbent surface area and pore shrinkage as nanoparticles agglomerate resulting in performance decay.[15] The operation was terminated after 100 cycles due to sorbent deterioration.

Zirconia was chosen as a sorbent stabilizer for its high Tammann temperature and refractory nature.[9] All Zr-incorporated CaO-based sorbents exhibited improved stability and performance compared to pure CaO (Figures 1 and 2). The addition of even half a mole of Zr to 10 mols of CaO (Zr/Ca=1/20) delayed sintering while maintaining molar conversions of 45% during the initial 100 cycles. Although the Zr/Ca (1/20) sorbent exhibited some initial deactivation, it showed good stability with increasing time. As expected, the stability of the CaO sorbent increased with increasing Zr doping.[9] However, drastic reduction in the sorption capacity of the Zr/Ca (6/10) was observed with an initial molar conversion of 38%, which is about 40% of the sorption capacity of pure CaO (Table 2). This huge reduction in molar conversion was attributed to the reduction of free CaO due to surface enrichment of Zr. The ability of sorbents to maintain high performance compared to our previous studies was credited to high concentration of CO_2 (99.5%) as the analysis gas and the use of a modified synthesis process resulting in uniform distribution of $CaZrO_3$ nanoparticles.[9,16] To better understand the effect of Zr doping on sorbent stability, all Zr-doped sorbents were examined under similar conditions, up to 250 cycles of operation. Only the sorbent with a molar ratio of 5/10 showed

Table 2. CaO Molar Conversion of Various FSP-Made Zr/Ca Nanosorbents after Various Cycles

Zr/Ca ratio	1st carbonation %	100th carbonation %	250th carbonation %	510th cycle	cycle started to decrease
0	95	30			6
1/20	92	45	32		~10
1/10	82	51	42		~25
2/10	79	68	45		~51
3/10	72	69	53		~90
4/10	65	65	62	50	~210
5/10	60	60	60	60	NO
6/10	38	38	38	38	NO

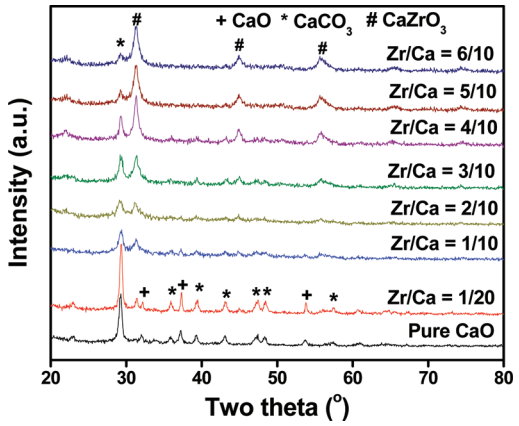

Figure 3. XRD patterns of the FSP-made pure and zirconia-doped CaO at various molar ratios of Zr/Ca.

excellent capacity and remarkable stability. The Zr/Ca (4/10) sorbent lost minimal activity (around 5%) during the 250 cycles of operation. Thus, these results confirm that Zr-loading improves the longevity of the sorbent.[9]

Further investigation on the durability and performance of the Zr/Ca (4/10, 5/10, and 6/10) sorbents was conducted, and the results are shown in Figure 2. The Zr/Ca (4/10) sorbent performance continued to deteriorate and reached about 46% molar conversion after 550 cycles, when the cyclic operation was terminated. But the other two sorbents showed superior resistance toward sintering after 1200 cycles. Even though the stability of the Zr/Ca (6/10) sorbent was similar to that of Zr/Ca (5/10), the molar conversion was nominal in contrast to the Zr/Ca (5/10) sorbent. Li et al.[17,18] reported molar conversion of 35% and 40% for $KMnO_4$-doped CaO and acetic acid modified limestone, respectively, during 100 cycles of carbonation−decarbonation operation. Similarly, Albrecht et al.[19] reported that MgO-doped CaO sorbents exhibited a molar conversion of only 28.1% during 1250 operating cycles. However, our FSP-made Zr/Ca (5/10) sorbent demonstrated a higher and better performance than those reported earlier[9] and exhibited 60% molar conversion during 1200 carbonation−decarbonation cycles, indicating a high potential for industrial applications.

3.3. Sorbent Characterization. The XRD patterns of FSP-made pure and zirconia-doped CaO are presented in Figure 3. The X-ray diffraction pattern of pure CaO exhibited reflections

Table 3. BET SSA and Pore Volumes of Various As Prepared and Spent FSP-Made Zr/Ca Sorbents with 1.5 mL min^{-1} Feed, 5 L min^{-1} Dispersion Gas, and 500/400 mL min^{-1} CH_4/O_2

sorbents	SSA (m^2/g)	spent sorbent SSA (m^2/g)	pore volume (cm^3/g)	$CaZrO_3$ crystal diameter (nm)	percentage perovskite phase (%)[b]
FSP 100% CaO	46		0.179		0
FSP Zr/Ca (1/20)	64		0.227	40.6	17
FSP Zr/Ca (1/10)	70		0.236	18.7	34
FSP Zr/Ca (2/10)	60		0.206	15.0	38
FSP Zr/Ca (3/10)	75	42	0.305	12.0	41
FSP Zr/Ca (4/10)	67	35	0.304	9.4	50
FSP Zr/Ca (5/10)	91	83	0.426	8.6	56
FSP Zr/Ca (6/10)	97		0.442	8.2	56
$CaO/CaZrO_3$ (55/45)[a]	4.4		0.016		
$CaO/CaZrO_3$ (50/50)[a]	6.5		0.027		
$CaO:CaZrO_3$ (45/55)[a]	7.0		0.024		

[a] Sorbents prepared by the physical mixing method. [b] Perovskite phase is attributed to $CaZrO_3$.

due to CaO (PDF-ICDD-00-004-0777) and $CaCO_3$ (PDF-ICDD-00-047-1743). The CaO peaks were also observed for the Zr/Ca (1:20) sorbent and disappeared upon further increase of Zr doping. All Zr-doped CaO sorbents exhibited a few more additional reflections at 31°, 45°, and 55°. These peaks primarily belong to $CaZrO_3$ (PDF-ICDD-00-035-0790). Their intensity increased with increasing Zr doping up to 5 mols. The $CaZrO_3$ is a perovskite with orthorhombic structure. It originates from the high temperature synthesis process that contributes to the sorbent resistance toward sintering.[20] The absence of a ZrO_2 crystal peak in the diffraction patterns indicates a complete incorporation of Zr into the CaO lattice during its synthesis. The improvement in mechanical stability of the synthesized sorbent, with increasing zirconia content for extended operation, is attributed to the perovskite phase (Table 3) as determined by

$$\text{Perovskite phase} = \frac{I_{\text{perov}}}{I_{\text{perov}} + I_{\text{CaO}} + I_{\text{CaCO}_3}} \times 100 \qquad (3)$$

where I represents the maximum intensity of each XRD crystal phase. The percentage of the perovskite phase of the sorbents increased with Zr addition and attained a maximum for the Zr/Ca molar ratio of 5/10. This percentage remained constant upon further zirconia addition that should cover the surface of free CaO, resulting in lower sorption capacity of the Zr/Ca (6/10) sorbent. The perovskite structure provides mechanical strength to the sorbents by acting as a barrier to CaO grain growth.[9] Table 3 shows that the $CaZrO_3$ crystallite size decreases with increasing zirconia loading. Therefore, these well-dispersed $CaZrO_3$ nanocrystals provide uniform stability to the sorbents during extended cyclic operation, which improved by increasing the zirconia doping.

The CO_2-TPD profiles of the as-prepared sorbents with different Zr/Ca molar ratios are presented in Figure 4. The CO_2-TPD profiles of pure CaO show that the desorption peak of chemisorbed CO_2 started at around 300 °C and reached maximum at 600 °C. This peak is due to the strong basic sites of CaO.[21,22] With increasing Zr loading, the desorption

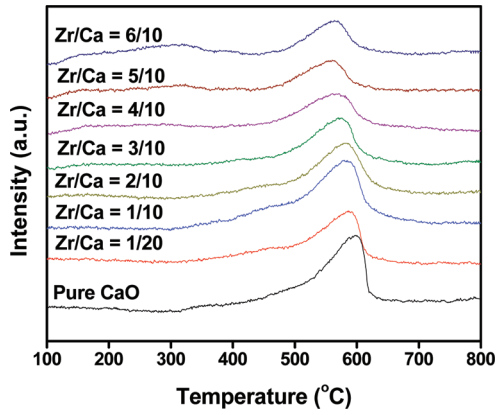

Figure 4. TPD analysis of CO_2 on various CaO-based sorbents.

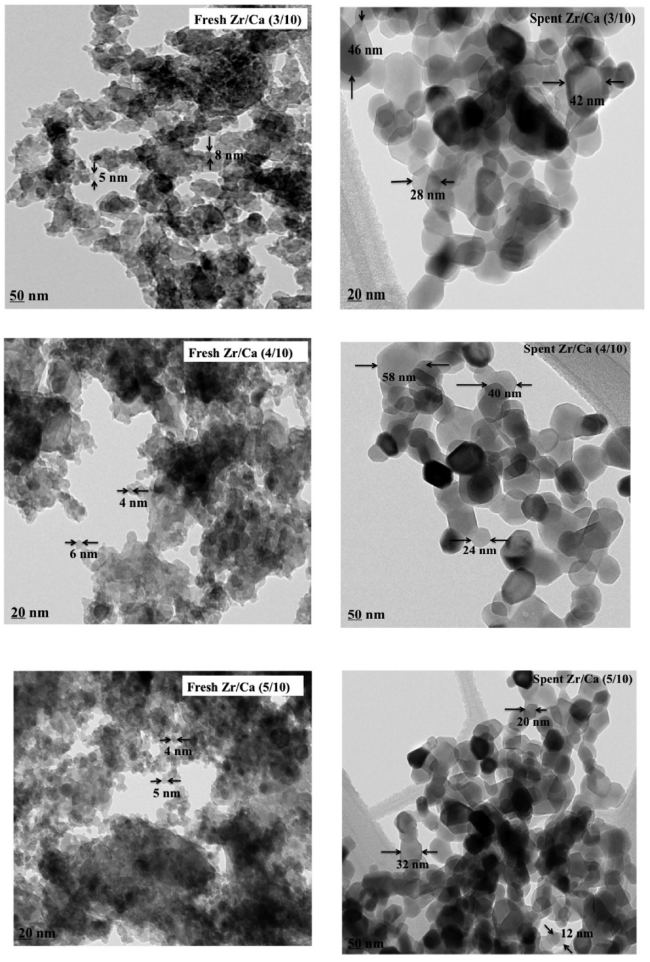

Figure 5. TEM images of various fresh and spent FSP-made Zr-doped CaO-based sorbents.

temperature for CaO continued to decrease. The shift of the major desorption peak position (600 to 560 °C) was attributed to the weak basic nature of zirconia.[21] This analysis suggests that weak basic natured zirconia covers the surface of strong basic sites of CaO, thus reducing the peak intensity contributed by CaO and forming a new low intensity peak at reduced temperature. This reduction in peak area with increasing zirconia doping is consistent with the reduction in sorbent sorption capacity. In addition to the major peak, a broad desorption peak between 200 and 300 °C appeared in Zr-doped samples. This peak is due to the desorption of CO_2 from weak basic sites of ZrO_2.[21]

Table 4. Binding Energy and Surface Atomic Ratios for Selected Sorbents As Determined by XPS

sample	O1s	Ca2p	Zr3d	Zr/Ca atomic ratio
CaO	532.5	348		Nd
Zr/Ca (3/10)	532.2	347.7	183	0.26
Zr/Ca (4/10)	531.5	347	181.7	0.35
Zr/Ca (5/10)	531.1	346.5	181.5	0.40
Zr/Ca (6/10)	531	346.5	181.5	0.53

The specific surface area (SSA) and pore volume of all FSP-made sorbents is shown in Table 3. Significant improvement of the SSA as well as the pore volume was observed with increasing zirconia doping. The increase in SSA and pore volume was attributed to the formation of nanocrystals of CaO, $CaCO_3$, and especially $CaZrO_3$ that hinders crystal growth during their high temperature synthesis. The SSA and pore volume of sorbents made by physical mixing were lower than the FSP-made sorbents. However, an increase in both SSA and pore volume was observed with increasing $CaZrO_3$ for the sorbents made by the physical mixing method. Thus, the presence of $CaZrO_3$ in these sorbents benefits their performance by increasing SSA and pore volume irrespective of their synthesis method.

The TEM images of selected fresh and spent Zr/Ca sorbents are presented in Figure 5. The images of fresh sorbents show a uniform distribution of nanoparticles. Particle sizes of the fresh sorbents are 4−8 nm. The Zr/Ca (5/10) sorbent exhibits the lowest particle size (4−5 nm) among the analyzed sorbents. The TEM images of spent sorbents show particle growth in all of them. The spent Zr/Ca (5/10) sorbent exhibited the lowest particle size growth (Figure 5). The TEM image of the spent Zr/Ca (5/10) sorbent shows the existence of a small proportion of particles with a maximum crystallite size observed around 32 nm after 1200 cycles of operation, whereas the TEM images of Zr/Ca (3/10) and Zr/Ca (4/10) mainly have particles with large crystallite sizes of 46 nm after 250 cycles and 58 nm after 510 cycles, respectively. The minimal increase of particle size for the Zr/Ca (5/10) sorbent after completion of the multicyclic operation can be attributed to the pretreatment temperature. The delay in particle size growth in all Zr/Ca sorbents is due to the increment in the formation of $CaZrO_3$ with increasing Zr loadings, which resists the sintering during the extended cycles of operation by forming a barrier between the CaO crystals.

In order to understand the nature of interactions between calcium and zirconium in the cubic fluorite (spinel) structure of CaO after Zr doping, selected Zr/Ca sorbents were subjected to XPS measurements. The photo electron peaks of O1s, Ca2p, and Zr3d of the sorbents are presented in Figures 6 and 7 and their corresponding electron binding energies are shown in Table 4. As presented in Figure 6, the O1s profile is, in general, broad and complicated due to the overlapping contribution of oxygen from calcia and zirconia.[23−25] It is obvious that the patterns are dominated by a broad peak at 532.5 eV attributed to the lattice oxygen associated with the calcium.[24] The gradual reduction in O1s binding energy with increasing Zr doping can be attributed

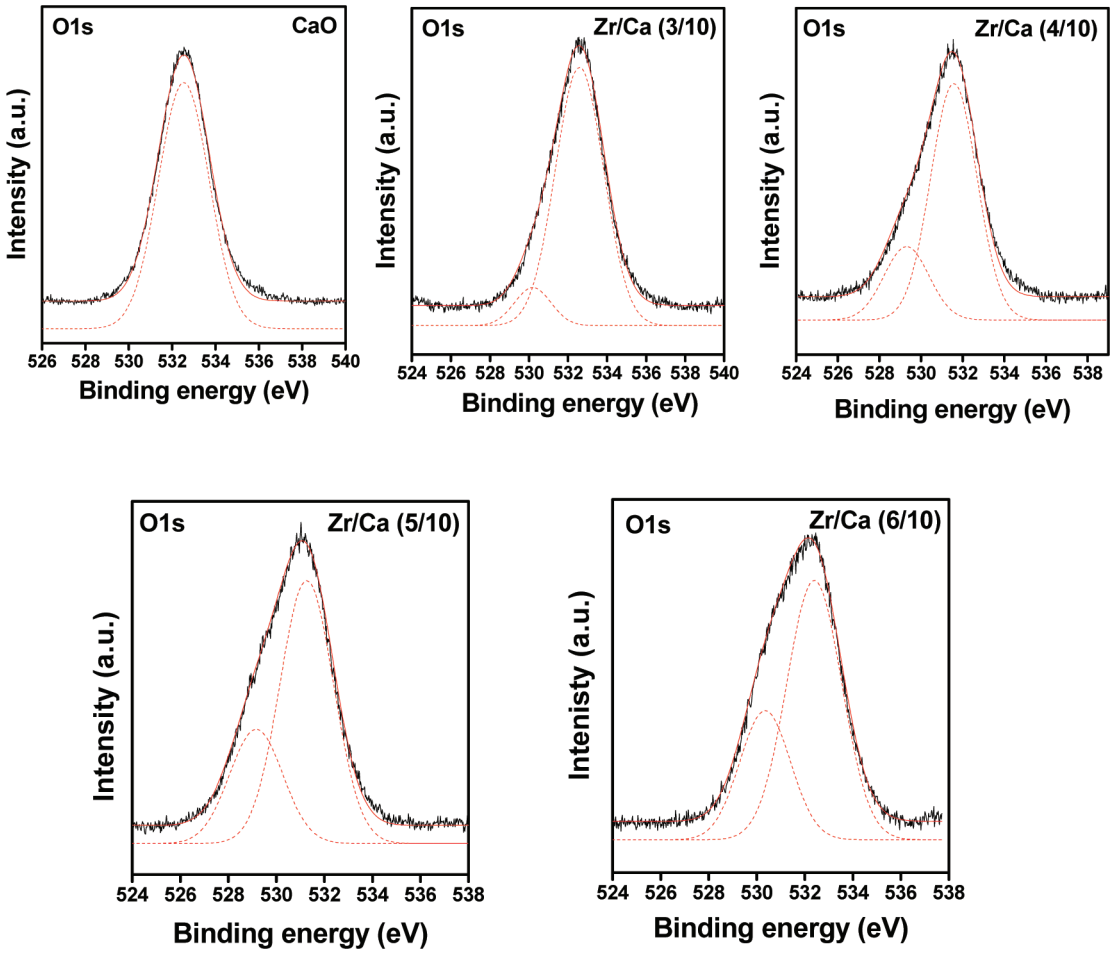

Figure 6. XPS spectra of O1s of pure and various zirconia-doped CaO sorbents.

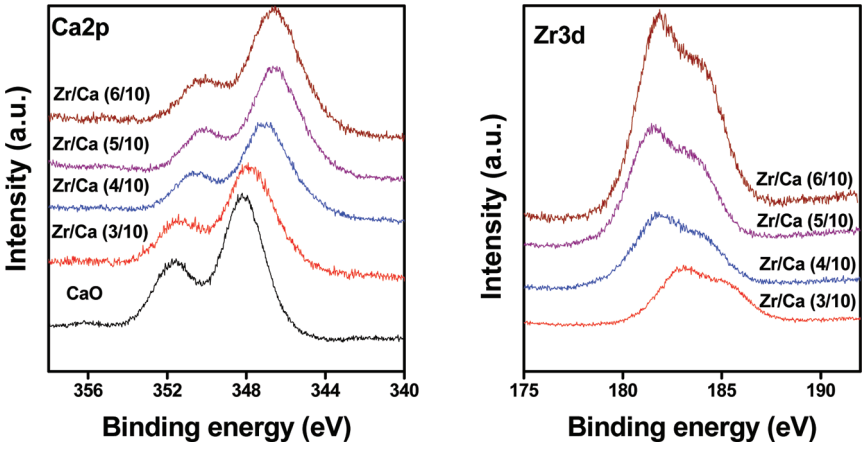

Figure 7. XPS spectra of Zr3d and Ca2p of pure and various zirconia-doped CaO sorbents.

to the increase of Zr content in the lattice of CaO. After Zr doping, an O1s peak bifurcation occurred giving an additional peak at 530.1 eV. Its intensity increased with increasing Zr content in the CaO sorbent. These results clearly indicate that there are two types of oxygen species on the surface of the Zr/Ca sorbents. The additional peak is due to the oxygen associated with the $CaZrO_3$. The present results are in good agreement with Reddy et al.[26] who also observed an additional peak in the O1s profile by the formation of $CeVO_4$ in $V_2O_5/CeO_2/Al_2O_3$ mixed oxides.

As shown in Figure 7 and Table 4, the Ca2p XPS spectra exhibit a peak at around 348 eV with a satellite peak at 351 eV, which could be attributed to the ionization of the $Ca2p_{3/2}$ and $Ca2p_{1/2}$ electrons of the Ca^{2+} oxidation state.[24] As expected, the intensity of Ca2p peak decreased with increasing Zr content. Interestingly, the binding energy of Ca2p decreased in the Zr/Ca (3/10) sorbent

dx.doi.org/10.1021/jp207625c |J. Phys. Chem. C 2011, 115, 24804–24812

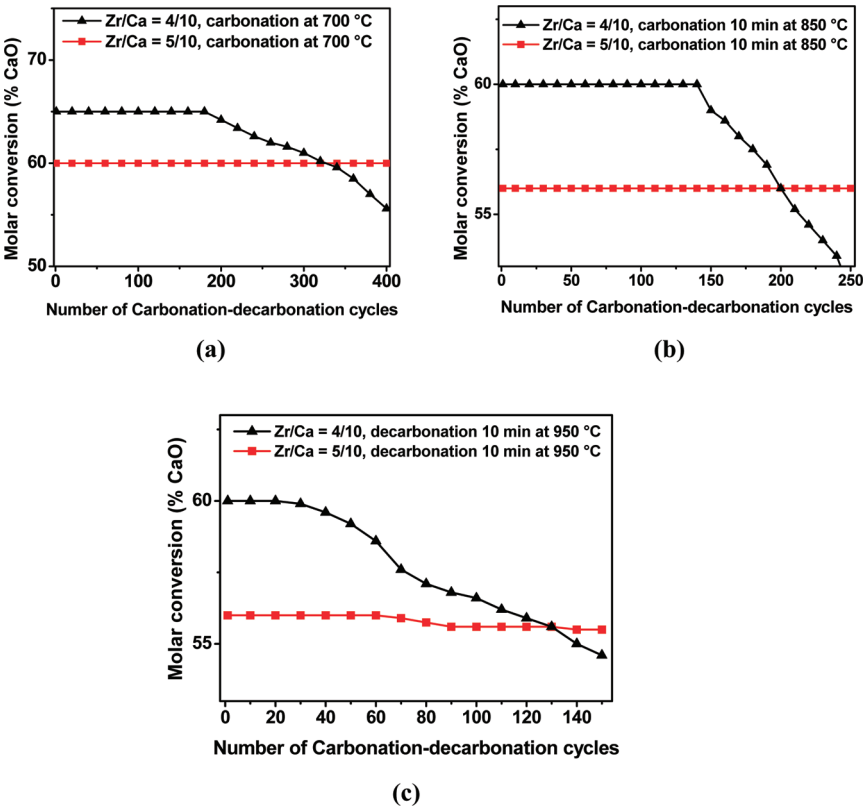

Figure 8. Effect of carbonation−decarbonation temperatures on molar conversion of Zr/Ca (4/10 and 5/10) sorbents during extended operating cycles. (a) Sorbents carbonated with 20 mL min^{-1} of CO_2 (99.5%) for 10 min at 700 °C and decarbonated for 10 min at 900 °C with 20 mL min^{-1} of helium. (b) The sorbents were carbonated with 20 mL min^{-1} of CO_2 (99.5%) for 10 min at 850 °C and decarbonated for 10 min at 900 °C with 20 mL min^{-1} of helium. (c) The sorbents were carbonated with 20 mL min^{-1} of CO_2 (99.5%) for 10 min at 850 °C and decarbonated for 10 min at 950 °C with 30 vol % CO_2 balanced helium.

compared to pure CaO, which was attributed to the formation of $CaZrO_3$. The Ca2p binding energy continued to decrease with increasing Zr content up to Zr/Ca = 5/10 and remained constant with the further addition of Zr. This behavior suggests that the formation of $CaZrO_3$ becomes maximum at that Zr content, in excellent agreement with the XRD results (Figure 3 and Table 3).

The Zr3d XPS spectra of Zr/Ca sorbets are presented in Figure 7, and the corresponding binding energies are presented in Table 4. The binding energy of the Zr3d photoelectron peak ranged between 183.2 and 184.6 eV, in agreement with the literature.[27] The core level spectra of Zr3d for the Zr/Ca sorbents showed an increasing intensity along with a shift toward lower binding energy with increasing Zr doping up to 5 mols of Zr per 10 mols of Ca. This indicates that the formation of $CaZrO_3$, whose quantity increased with increasing Zr doping, reaching a maximum at Zr/Ca (5/10). The Zr/Ca atomic ratios as determined by XPS are presented in Table 4. As expected, Zr/Ca atomic ratios increased with increasing Zr content. Interestingly, by increasing the Zr doping from 3 mols to 5 mols, the Zr/Ca atomic ratio increased from 0.26 to 0.4, while further doping of Zr (from 5 mols to 6 mols of Zr) increased the atomic ratio from 0.4 to 0.53. These results suggest that further doping of Zr into the Zr/Ca (5/10) sorbent leads to no additional formation of $CaZrO_3$. Moreover, this implies that surface enrichment of zirconium takes place on the surface, thus decreasing the amount of free CaO. This is the reason why there is a sharp decrease in capture capacity when Zr content is increased from 5 to 6 mols during our extended carbonation−decarbonation cycles.

3.4. Effect of Severe Conditions on Sorbent Performance.

3.4.1. Effect of Carbonation and Decarbonation Temperature. Both 4/10 and 5/10 Zr/Ca sorbents are investigated under high decarbonation temperatures. The analysis was performed at a carbonation temperature of 700 °C with a flow rate of 20 mL min^{-1} of CO_2 (99.5%) for 10 min and decarbonation at 900 °C in helium. Both sorbents showed excellent resistance toward sintering at high temperatures (Figure 8a). The Zr/Ca (5/10) sorbent showed no signs of deactivation up to 250 carbonation−decarbonation cycles. This enhanced thermal stability of the sorbent over a wide range of decarbonation temperatures is accounted for by the broadening of the temperature window. Further analysis of these sorbents was performed to investigate the effect of high carbonation temperature (850 °C) on the sorption capacity and stability (Figure 8b). The performance of Zr/Ca sorbents with molar ratios of 4/10 and 5/10 at a higher carbonation temperature (850 °C) was reduced compared to that at low carbonation temperature (700 °C). The reduction in sorption capacity was due to the dominance of decarbonation over carbonation as well as pore shrinkage and reduction in surface area, which are driven by high temperatures.[28,29]

Introduction of concentrated CO_2 at a high carbonation temperature results in a $CaCO_3$ layer on the surface of CaO. This layer changes the capture process from being reaction-controlled to diffusion-controlled. A high carbonation temperature also increases the CaO crystal size. The performance of the Zr/Ca (4/10) sorbents during carbonation at 850 °C started to decline after 140 cycles. This suggests that sorbent stability can be significantly hindered by high CO_2 concentration at high

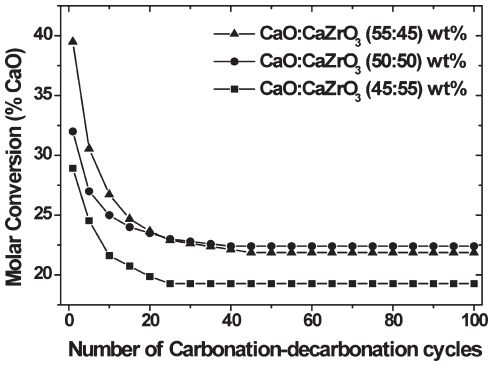

Figure 9. Extended operation cycles of sorbents from physical mixing. The sorbents were carbonated for 10 min at 700 °C, and decarbonation was performed by raising the temperature to 800 °C and back to the carbonation temperature in helium.

temperatures. However, the Zr/Ca (5/10) sorbent exhibits excellent resistance toward sintering even at a high carbonation temperature, indicating good potential to be used in harsh environments.

3.4.2. Performance of Zr/Ca Sorbents during Extended Operating Cycles. Further investigations were conducted with the Zr/Ca (4/10 and 5/10) sorbents with carbonation at 850 °C in pure CO_2 (99.5% purity) and decarbonation at 950 °C in 30 vol % of CO_2 balanced helium. These results are presented in Figure 8c, which also depicts the occurrence of early deactivation of the Zr/Ca (4/10) sorbent. Interestingly, the Zr/Ca (5/10) sorbent exhibits optimum performance up to 150 operating cycles. This notable stability and appreciable performance of the Zr/Ca (5/10) sorbent in the hostile environment shows that $CaZrO_3$ provides significant resistance to particle growth. These properties make Zr/Ca (5/10) a very promising sorbent for industrial applications among all the synthesized sorbents for extended carbonation−decarbonation cycles.

3.5. Evaluation of Sorbents Derived from Physical Mixing. All sorbents from physical mixing exhibited lower molar conversion than FSP-made sorbents, which is attributed to the low surface areas and pore volumes of the former sorbents (Figure 9). In the early stages of operation, a reduction in sorption capacity was observed on all sorbents, which stabilized as the operation cycles proceeded. The early decline of CO_2 capture capacity was attributed to sintering of commercial CaO,[30] which was prevented by $CaZrO_3$ nanoparticles during later operation cycles. A significant reduction in molar conversion was observed with the higher $CaZrO_3$ incorporation. Therefore, optimal combination of CaO and $CaZrO_3$ in the physical mixing method is required to produce highly durable sorbents.

3.6. Role of $CaZrO_3$ Formation on Stability and Performance of Sorbents. All characterization measurements suggest that calcium zirconate ($CaZrO_3$) was formed in all flame-made Zr-doped CaO-based sorbents. The flame process favors formation of $CaZrO_3$, which creates a barrier between CaO grains, thus preventing the sintering-agglomeration leading to improved sorbent performance.[31] When the total molar conversion for free CaO particles in Zr-doped CaO sorbents is calculated, the Zr/Ca (5/10) sorbent exhibited much more capture capacity than all others. Therefore, the formation of $CaZrO_3$ not only stabilizes the CaO particles but also increases their CO_2 capture capacity. However, even though the Zr/Ca (6/10) sample exhibits an equal amount of $CaZrO_3$, the molar conversion for the free CaO particles is less than that for the Zr/Ca (5/10) sorbent. The XRD and XPS suggest that the formation of $CaZrO_3$ attains a maximum value at a Zr/Ca molar ratio of 5/10 and remains constant upon any further increase in molar ratio. When increasing the Zr-doping from 5 to 6 mols, it forms an amorphous ZrO_2 layer over the CaO surface. The XPS results support this observation. These results are consistent with flame synthesis of SiO_2-doped TiO_2,[32] where after a certain Si-doping level, a rich SiO_2 layer forms on the TiO_2 surface. Hence, the lower capture capacity of the Zr/Ca (6/10) sorbent is probably due to the formation of the amorphous ZrO_2 layer over the CaO surface.

The formed $CaZrO_3$ is a perovskite with an orthorhombic structure. The $CaZrO_3$ is superior to ZrO_2 since it possesses a relatively high melting temperature (~2345 °C), thermal and chemical stability, good thermal shock resistance, and relatively low thermal expansion coefficient.[33,34] Therefore, the CaO sorbents with ZrO_2 (made by the wet method at low calcination temperatures) exhibit lower thermal resistance, thus resulting in early decay in stability irrespective of the high Tammann temperature.[9] An increase in the perovskite phase ($CaZrO_3$) content with increasing Zr loading on CaO was observed (Figure 3 and Table 3). The sorbent stability improves with increasing the $CaZrO_3$ content, and the Zr/Ca (5/10) sorbent shows excellent capture capacity and remarkable stability during prolonged cyclic carbonation−decarbonation.

The TEM study of spent sorbents reveals there is an increase in crystallite size of CaO after CO_2 capture analysis. Even though TEM is a good technique to study the particle morphology, it is difficult to accurately measure the average crystallite size. Hence, we performed BET surface area measurements over the spent sorbents to investigate the particle surface area after the CO_2 capture analysis. Interestingly, the Zr/Ca (5/10) sorbent surface area decreased only from 91 m^2/g to 83 m^2/g. However, the other sorbents Zr/Ca (3/10) and Zr/Ca (4/10) surface areas decreased from 75 and 67 m^2/g to 42 and 35 m^2/g, respectively. These results suggest that the formation of the optimum $CaZrO_3$ amount stabilizes the CaO particles against sintering during CO_2 capture for extended cycles in the Zr/Ca (5/10) sorbent. Even though significant stability was observed, a very low capture capacity was observed for the Zr/Ca (6/10) sorbent.

4. CONCLUSIONS

The FSP-made Zr/Ca sorbent with the molar ratio of 5/10 exhibits excellent CO_2 capture capacity and magnificent stability among all Zr-doped CaO-based sorbents during extended operating cycles. According to XPS, there is no significant change in the oxidation state of Ca^{2+} on doping with zirconium. XPS and XRD results also show that for Zr/Ca ratios higher than 0.5, the addition of Zr does not lead to additional $CaZrO_3$, and in fact, surface enrichment of zirconium takes place, which decreases the free CaO for CO_2 capture. As a result, a sharp decrease in capture capacity of the Zr/Ca (6/10) sorbent was observed.

The enhanced performance of the optimally doped sorbent, Zr/Ca (5/10), can be attributed to well-dispersed $CaZrO_3$ nanoparticles as well as a high specific surface area and large pore volume. The performance of sorbents remained unaffected when tested under a high decarbonation temperature of 900 °C. Even under these severe conditions, the Zr/Ca (5/10) sorbent maintained excellent stability and optimal performance for 150 cycles. This resistance to sintering at high temperatures is attributed to the $CaZrO_3$ nanoparticles, which act as an inert barrier preventing agglomeration of CaO particles. The TEM

images also show minimal particle size growth in the sorbents with higher $CaZrO_3$ content during extended operating cycles.

The optimal performance of the sorbent was achieved by controlling the combination of CaO and $CaZrO_3$ as well as their particle sizes. Properties like high melting point, good thermal shock resistance, and the low thermal expansion coefficient of $CaZrO_3$ provide a major boost to the sorbent stability. On the whole, the present study concludes that for extended industrial multicycle operations, the Zr/Ca sorbent with the molar ratio of 5/10 will be the best choice due to its excellent and stable performance.

AUTHOR INFORMATION

Corresponding Author

*Tel: (513) 556-1474. Fax: (513) 556-3473. E-mail: panagiotis.smirniotis@uc.edu.

ACKNOWLEDGMENT

We thank Dr. Rodica B. McCoy and Dr. Jacek Jasinski of the materials characterization laboratories of the University of Kentucky at Louisville for helping with the XPS measurements.

REFERENCES

(1) Zhou, Q.; Chan, C.; Tontiwachiwuthikul, P. Monitoring and Diagnosis of the Carbon Dioxide Capture Process Using an Intelligent System Approach. *Procedia Environ. Sci.* **2010**, *2*, 2–8.

(2) Chew, J.-L.; Ahmad, A. L.; Bhatia, S. Ordered Mesoporous Silica (OMS) As an Adosrbent and Membrane for Separation of Carbon Dioxide (CO_2). *Adv. Colloid Interface Sci.* **2010**, *153*, 43–57.

(3) Liu, W.; Low, N. W.; Feng, B.; Wang, G.; Costa, D. D. Calcium Precursors for the Production of CaO Sorbents for Multicycle CO_2 Capture. *Environ. Sci. Technol.* **2010**, *44*, 3093–3097.

(4) Arias, B.; Grasa, G. S.; Abanad, J. C. Effect of Sorbent Hydration on the Average Activity of CaO in a Ca-Looping Systemq. *Chem. Eng. J.* **2010**, *163*, 324–330.

(5) Manovic, V.; Anthony, E. J. Steam Reactivation of Spent CaO-Based Sorbent for Multiple CO_2 Capture Cycles. *Environ. Sci. Technol.* **2007**, *41*, 1420–1425.

(6) Martavaltzi, C. S.; Lemonidou, A. A. Development of New CaO Based Sorbent Materials for CO_2 Removal at High Temperature. *Microporous Mesoporous Mater.* **2008**, *110*, 119–127.

(7) Li, S.-Z.; Cai, S.-N.; Huang, Y.-Y.; Han, J.-H. Effect of Preparation Temperature on Cyclic CO_2 Capture and Multiple Carbonation−Calcination Cycles for a New Ca-Based CO_2 Sorbent. *Ind. Eng. Chem. Res.* **2006**, *45*, 1911–1917.

(8) Aihara, M.; Nagai, T.; Matsushita, J.; Negishi, Y.; Ohya, H. Development of Porous Solid Reactant for Thermal-Energy Storage and Temperature Upgrade Using Carbonation/Decarbonation Reaction. *Appl. Energy* **2001**, *69*, 225–238.

(9) Lu, H.; Khan, A.; Pratsinis, S. E.; Smirniotis, P. G. Flame-Made Durable Doped-CaO Nanosorbents for CO_2 Capture. *Energy Fuels* **2009**, *23*, 1093–1100.

(10) Rudin, T.; Wegner, K.; Pratsinis, S. E. Uniform Nanoparticles by Flame-Assisted Spray Pyrolysis (FASP) of Low Cost Precursors. *J. Nanopart. Res.* **2011**, *13*, 2715–2725.

(11) Klug, H. P.; Alexander, L. E. *X-ray Diffraction Procedures for Polycrystalline and Amorphous Materials*, 2nd ed.; Wiley: New York, 1974.

(12) Mädler, L.; Kammler, H. K.; Mueller, R.; Pratsinis, S. E. Controlled Synthesis of Nanostructured Particles by Flame Spray Pyrolysis. *J. Aerosol Sci.* **2002**, *33*, 369–389.

(13) Tani, T.; Mädler, L.; Pratsinis, S. E. Homogeneous ZnO Nanoparticles by Flame Spray Pyrolysis. *J. Nanopart. Res.* **2002**, *4*, 337–343.

(14) Mädler, L.; Stark, W. J.; Pratsinis, S. E. Flame-Made Ceria Nanoparticles. *J. Mater. Res.* **2002**, *17*, 1356–1362.

(15) Abanades, J. C.; Alvarez, D. Conversion Limits in the Reaction of CO_2 with Lime. *Energy Fuels* **2003**, *17*, 308–315.

(16) Luo, C.; Zheng, Y.; Ding, N.; Wu, O.; Bian, G.; Zheng, C. Development and Performance of CaO/La_2O Sorbents during Calcium Looping Cycles for CO_2 Capture. *Ind. Eng. Chem. Res.* **2010**, *49*, 11778–11784.

(17) Li, Y.; Zhao, C.; Chen, H.; Duan, L.; Chen, X. Cyclic CO_2 Capture Behavior of $KMnO_4$-Doped CaO-Based Sorbent. *Fuel* **2010**, *89*, 642–649.

(18) Li, Y.; Zhao, C.; Chen, H.; Liu, Y. Enhancement of Ca-Based Sorbent Multicyclic Behavior in Ca Looping Process for CO_2 Separation. *Chem. Eng. Technol.* **2009**, *32*, 548–555.

(19) Albrecht, K. O.; Wagenbach, K. S.; Satrio, J. A.; Shanks, B. H.; Wheelock, T. D. Development of a CaO-Based CO_2 Sorbent with Improved Cyclic Stability. *Ind. Eng. Chem. Res.* **2008**, *47*, 7841–7848.

(20) Róg, G.; Dudek, M.; Kozlowska-Róg, A.; Buć ko, M. Calcium-zirconate: Preparation, Properties and Application to the Solid Oxide Galvanic Cells. *Electrochim. Acta* **2002**, *47*, 4523–4529.

(21) Liu, S.; Ma, J.; Guan, L.; Li, J.; Wei, W.; Sun, Y. Mesoporous $CaO-ZrO_2$ Nano-Oxides: A Novel Solid Base with High Activity and Stability. *Microporous Mesoporous Mater.* **2009**, *117*, 466–471.

(22) Istadi; Amin, N. A. S. Synergistic Effect of Catalyst Basicity and Reducibility on Performance of Ternary CeO_2-Based Catalyst for CO_2 OCM to C_2 Hydrocarbons. *J. Mol. Catal A: Chem.* **2006**, *259*, 61–66.

(23) Sawatzky, G. A.; Post, D. X-ray Photoelectron and Auger Spectroscopy Study of Some Vanadium Oxides. *Phys. Rev. B* **1979**, *20*, 1546–1555.

(24) Wagner, C. D.; Riggs, W. M.; Davis, L. E.; Moulder, J. F. In *Handbook of X-ray Photoelectron Spectroscopy*; Muilenberg, G. E., Ed.; Perkin-Elmer Corp.: Waltham, MA, 1978.

(25) Imamura, I.; Ishida, S.; Taramoto, H.; Saito, Y. *J. Chem. Soc., Faraday Trans.* **1993**, *89*, 757.

(26) Reddy, B. M.; Rao, K. N.; Reddy, G. K.; Park, S. E. Structural Characterization and Oxidehydrogenation Activity of CeO_2/Al_2O_3 and $V_2O_5/CeO_2/Al_2O_3$ Catalysts. *J. Phys. Chem. C* **2007**, *111*, 18751–18758.

(27) Reddy, B. M.; Reddy, G. K.; Rao, K. N.; Katta, L. Influence of Alumina and Titania on the Structure and Catalytic Properties of Sulfated Zirconia: Beckmann Rearrangement. *J. Mol. Catal. A: Chem.* **2009**, *306*, 62–68.

(28) Ma, W.-K.; Teng, H. CaO Powders from Oyster Shells for Efficient CO_2 Capture in Multiple Carbonation Cycles. *J. Am. Ceram. Soc.* **2010**, *93*, 221–227.

(29) Sun, P.; Lim, J. C.; Grace, J. R. Cyclic CO_2 Capture by Limestone-Derived Sorbent During Prolonged Calcination/Carbonation Cycling. *AIChE J.* **2008**, *54*, 1668–1677.

(30) Li, L.; King, D. L.; Nie, Z.; Howard, C. Magnesia-Stabilized Calcium Oxide Absorbents with Improved Durability for High Temperature CO_2 Capture. *Ind. Eng. Chem. Res.* **2009**, *48*, 10604–10613.

(31) Manik, K. S.; Pradhan, K. S. X-ray Microstructure Characterization of Ball-Milled Nanocrystalline Microwave Dielectric $CaZrO_3$ by Rietveld Method. *Appl. Crystallogr.* **2005**, *38*, 291–298.

(32) Akhtar, M. K.; Pratsinis, S. E.; Mastrangelo, V. R. Dopants in Vapor-Phase Synthesis of Titania Powders. *J. Am. Ceram. Soc.* **1992**, *75*, 3408–3416.

(33) Pretis, D.; Ricciardiello, F.; Sbaizero, O. Mechanical Properties of Polycrystalline $CaZrO_3$. *Powder Metall. Int.* **1986**, *18*, 427–430.

(34) Thongtha, A.; Laowanidwatana, A.; Bongkarn, T. Effect of Firing Temperatures on Phase and Morphology Evolution of $CaZrO_3$ Ceramics Synthesized Using the Combustion Technique. *Ferroelectrics* **2010**, *403*, 3–10.